

000 001 002 003 004 005 006 007 008 009 010 011 012 013 014 015 016 017 018 019 020 021 022 023 024 025 026 027 028 029 030 031 032 033 034 035 036 037 038 039 040 041 042 043 044 045 046 047 048 049 050 051 052 053 GENERALIZABLE COARSE-TO-FINE ROBOT MANIPULATION VIA LANGUAGE-ALIGNED 3D KEYPOINTS

Anonymous authors

Paper under double-blind review

ABSTRACT

Hierarchical coarse-to-fine policy, where a coarse branch predicts a region of interest to guide a fine-grained action predictor, has demonstrated significant potential in robotic 3D manipulation tasks by especially enhancing sample efficiency and enabling more precise manipulation. However, even augmented with pre-trained models, these hierarchical policies still suffer from generalization issues. To enhance generalization to novel instructions and environment variations, we propose Coarse-to-fine Language-Aligned manipulation Policy (CLAP), a framework that integrates three key components: 1) task decomposition, 2) VLM fine-tuning for 3D keypoint prediction, and 3) 3D-aware representation. Through comprehensive experiments in simulation and on a real robot, we demonstrate its superior generalization capability. Specifically, on GemBench, a benchmark designed for evaluating generalization, our approach achieves a 12% higher average success rate than the SOTA method while using only 1/5 of the training trajectories. In real-world experiments, our policy, trained on only 10 demonstrations, successfully generalizes to novel instructions and environments.

1 INTRODUCTION

Robot learning, especially via imitation learning, has demonstrated promising success in enabling robots to solve complex 3D manipulation tasks (Intelligence et al., 2025; Liu et al., 2024). However, scaling these methods to a broader range of real-world applications (e.g., industrial, service, or home robotics) requires enhancing both (G1) their generalization to environment variations, and (G2) their skill compositional generalization. Indeed, G1 is necessary, because deployed robots need to be able to operate in new settings (e.g., object or background variation), while G2 is highly desirable, so that trained robots can tackle new tasks by composing previously-learned skills. To achieve G1 and G2, the robot needs to be endowed with a combination of capabilities, such as scene understanding, reasoning or planning, and high-precision manipulation, exploiting preferably sample efficient techniques, since robotics data is costly to collect.

In this paper, we focus on one type of 3D manipulation policies, called *coarse-to-fine* policies (Gualtieri & Platt, 2020; James et al., 2022; Ling et al., 2024; Goyal et al., 2024; Gervet et al., 2023; Liu et al., 2025), because they achieve superior precision in manipulation tasks while enjoying strong sample efficiency. These policies process 3D observations (or 3D scene representations) using a hierarchical architecture whose higher-level coarse branch identifies a region of interest for the lower-level fine-grained branch to focus on and predict a final action. Typically, the coarse branch is trained to predict a 3D keypoint, which serves as the center for cropping and zooming into the original 3D observations. To help with visual understanding and to some extent spatial reasoning, recent work (Li et al., 2025b; Fang et al., 2025) has extended this approach to exploit pre-trained models—Vision-Language Models (VLMs) (Beyer et al., 2024) or visual foundation models (Ravi et al., 2024). However, the performance of these obtained methods is still limited in terms of generalization capability (G1 and especially G2), indicating that their scene understanding and reasoning capabilities are actually still rudimentary. Our experimental study suggests that this is primarily due to a combination of various issues (depending on the method), such as domain shift between pre-training and robotic images, inadequacy of pre-trained models to predict 3D keypoint, poor adaptation to object variations, or under-exploitation of the planning ability of VLMs.

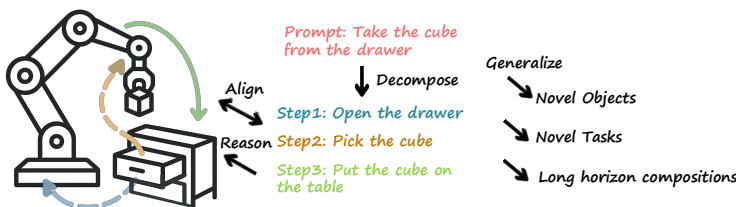


Figure 1: **Intuition of CLAP.** Our method achieves strong generalization ability by decomposing tasks into step-wise language instructions, each aligned with a 3D keypoint.

To address these limitations and issues, we propose Coarse-to-fine Language-Aligned manipulation Policy (**CLAP**), a novel coarse-to-fine 3D manipulation policy. In contrast to previous coarse-to-fine policies, CLAP includes a novel architecture for the higher-level branch, which we name *coarse task planner*, and a novel implementation of the lower-level fine-grained action predictor, both leveraging pre-trained models.

The coarse task planner, implemented as a VLM, is introduced to play the additional role of task planning. Before the usual 3D keypoint prediction, it decomposes a task into step-wise language instructions, representing basic skills. This change allows both 3D keypoint and action predictions to depend on step-wise instructions instead of the whole task description, which promotes skill compositional generalization (G2). The training of this coarse task planner consists of three parts to reinforce its scene understanding and reasoning capabilities. First, the pre-trained VLM fine-tuned on language plans of different tasks to directly improve compositional reasoning. Second, it is specialized for 3D keypoint prediction by fine-tuning it to perform a sequential reasoning process: first localizing task-related objects, then generating the step instruction, and finally predicting a corresponding 3D keypoint. Finally, to further boost its scene understanding capability, the VLM is further fine-tuned with an auxiliary task of 3D object detection, using an additional dataset of object positions. Together, these components form a comprehensive pipeline that significantly enhances the generalization ability of the coarse-to-fine policy to object variations (G1) and novel tasks (G2).

The fine-grained action predictor takes as input both the step instruction and the multi-view RGB-D images and outputs an action. It is implemented with specialized pre-trained models to improve sample efficiency and increase its precision during manipulation. More specifically, step instruction and RGB images are processed using a pre-trained visual-language encoder, ensuring the two modalities are well-aligned. The depth information is processed by a dedicated encoder and augmented with 3D position embeddings to help better align 3D and 2D image information. All the obtained embeddings, which we call 3D-aware representation, are fused via a Multi-View Transformer (Goyal et al., 2023) to predict the final actions.

To evaluate the performance of our method, we run experiments in both simulation and real-world. For simulation, we use GemBench (Garcia et al., 2025), a benchmark specifically designed to assess the generalization ability of multi-task language-conditioned policies across varying difficulty levels. Our approach outperforms the state-of-the-art method, achieving a 12% higher average success rate with only 1/5 of the training trajectories. In real-world experiments, our method demonstrate strong generalization ability to novel tasks and object variations with only 10 demonstrations per task.

Contributions

1. We introduce a novel coarse-to-fine 3D manipulation policy, as shown in Figure 1, with two main innovations: (1) tasks are decomposed into step-wise language instructions to promote compositional generalization ability; (2) action inference is performed via a reasoning step to improve generalization to object variations.
2. We design a finetuning pipeline that effectively adapts a pre-trained VLM to 3D keypoint prediction and incorporate a 3D-aware representation in the fine-grained action predictor, overcoming the issues observed in previous methods.
3. Empirical evaluations in simulation and on a real robot demonstrate state-of-the-art performance in both robustness to visual and object changes and generalization to unseen tasks.

108
109
110
2 RELATED WORK111
112
In this section, we discuss the related works in the field, including vision-language-action models,
3D manipulation policies, and coarse-to-fine policies.113
114
Vision-Language-Action (VLA) models Training VLMs (OpenAI, 2024; Beyer et al., 2024; Bai
115 et al., 2025; AI, 2024) on vast internet-scale image-text corpora has led to remarkable capabilities
116 in image understanding, excelling at tasks like image classification, object detection, and visual
117 question answering tasks. However, applying a similar training strategy directly to robotics presents
118 a challenge due to the relatively scarce robot trajectory data. A prominent solution is to transfer
119 the knowledge from pre-trained VLMs by fine-tuning them on robot data. This approach is the
120 foundation for recent VLA models (Driess et al., 2023; Brohan et al., 2023; Kim et al., 2024; Octo
121 Model Team et al., 2024; Intelligence et al., 2025; Wen et al., 2025a; Shukor et al., 2025; Liu et al.,
122 2024; Wen et al., 2025b; Li et al., 2024; Cheang et al., 2025; Team et al., 2025; NVIDIA et al.,
123 2025), which are fine-tuned on large diverse datasets of robot trajectories. Such extensive training
124 strengthens generalization to novel objects, environments, and tasks. However, since they commonly
125 use multi-view 2D images as visual input, learning to reason in 3D space from 2D images alone is
126 data-intensive. This leads to sample inefficiency and low success rates on some tasks. Recent
127 work has sought to more explicitly incorporate 3D information (Li et al., 2025a; Qu et al., 2025;
128 Zhen et al., 2024) or introduce Chain of Thought (Mu et al., 2023; Zawalski et al., 2024; Zhao et al.,
129 2025) to enhance the 3D reasoning ability. However these directions remain relatively underexplored
130 within the VLA paradigm. Our method, which fine-tunes a pretrained VLM as a coarse task planner
131 and predicts the final action with a fine-grained action predictor, can also be viewed as a VLA
132 model. In contrast to other VLA approaches, we propose specific training and inference techniques
133 to better align pre-trained VLMs to 3D manipulation, further enhancing generalization (G1-G2)
134 while retaining the sample efficiency inherent to hierarchical coarse-to-fine policies.135
136
3D Manipulation Policy 3D manipulation policies (Shridhar et al., 2022; Gervet et al., 2023; Jia
137 et al., 2025; Zhu et al., 2025; Wang et al., 2024b; Ze et al., 2024; Wang et al., 2024a; Goyal et al.,
138 2024; Ke et al., 2024; Chen et al., 2025a;b; Fang et al., 2025; Li et al., 2025b; Garcia et al., 2025)
139 directly work with 3D inputs and outputs. They generally include structured architectures that
140 construct a 3D representation of the scene, leading to higher sample efficiency and better generalization
141 to new camera viewpoints. For example, PerAct (Shridhar et al., 2022) explicitly represents the
142 scene with a voxel representation. Gervet et al. (2023) and Ke et al. (2024) process RGB images
143 with pre-trained image encoder and lift 2D features to 3D by aggregating with depth information.
144 An alternative approach (Jia et al., 2025; Goyal et al., 2024) is to project point clouds into canonical
145 virtual views and use the resulting multi-view images as input. Explicitly exploiting 3D information
146 allows these models to achieve high success rates with much less training data, which can be further
147 reduced by enforcing a hierarchical structure like in coarse-to-fine policies.148
149
Coarse-to-fine Policies Gualtieri & Platt (2018; 2020) first propose this coarse-to-fine scheme
150 for pick-and-place tasks. Subsequent work has considered more general tasks and explored various
151 3D representations, such as voxel observations (James et al., 2022; Liu et al., 2025), 3D feature
152 fields (Gervet et al., 2023), and multi-view images (Goyal et al., 2024). Ling et al. (2024) apply the
153 coarse-to-fine architecture to handle noisy point clouds. Among these, Robotic View Transformer
154 2 (RVT2) (Goyal et al., 2024) is an effective language-conditioned multi-task policy, demonstrating
155 strong performance in both training and inference efficiency by using multi-view images projected
156 from canonical views. However, RVT2 is trained from scratch, which limits its generalization ability
157 to visual perturbations and task variations. Subsequent efforts built upon this work have sought to
158 overcome these limitations. Existing works (Li et al., 2025b; Fang et al., 2025) have attempted to
159 enhance generalization through strategies such as: pre-training on object detection datasets (Yuan
160 et al., 2024) or integrating encoders from powerful visual foundation models like Segment Anything
161 Model 2 (Ravi et al., 2024). In contrast, we achieve this by introducing a novel architecture, where
162 tasks are decomposed into step-wise language instructions for skill compositional generalization and
163 design a specific training and inference pipeline to leverage pre-trained models in both coarse and
164 fine-grained branches.

162

3 BACKGROUND

164 In this section, we first briefly recall the multi-task imitation learning set-up, introduce coarse-to-fine
 165 policy, and then present Robotic-View-Transformer 2 (RVT2) (Goyal et al., 2024), a state-of-the-art
 166 coarse-to-fine policy that serves as the foundation for our method.

167 In multi-task imitation learning, a dataset $\mathcal{D} = \{(\tau_i, L_i) \mid i = 1, \dots, N\}$ is available for pairs
 168 of robot demonstrations τ_i and task description L_i . A robot demonstration is a trajectory $\tau_i =$
 169 $(o_0, a_0, o_1, a_1, \dots)$ containing a sequence of observations o_t and corresponding expert actions a_t .
 170 Observations include multi-view RGB-D images and gripper status indicating whether it is close or
 171 open. Actions denote the state of the end-effector, which contains the 3D position $p_t = (x_t, y_t, z_t)$
 172 of the gripper, the orientation of the gripper and a gripper status.

173 A coarse-to-fine policy contains a coarse branch and a fine-grained branch, where the coarse branch
 174 predicts a 3D keypoint as the center to zoom in the 3D observation and the fine-grained branch
 175 uses the refined observation to predict the target action. Such policy is trained according to the
 176 key-frame based imitation learning framework (Johns, 2021; Shridhar et al., 2022; Goyal et al.,
 177 2024). Specifically, key-frames identifies timesteps in a trajectory when an important action, like
 178 grasping or placing, occurs. In practice, they are usually heuristically defined for each trajectory.
 179 With these key-frames, a trajectory is segmented into K subsequences of observations and actions
 180 $(o_0, a_0, \dots, o_{t_1}, a_{t_1}), \dots, (o_{t_{K-1}+1}, a_{t_{K-1}+1}, \dots, o_{t_K}, a_{t_K})$, where the k^{th} key-frame occurs at time
 181 step t_k , from which we can extract a sequence of key-frame actions $(a_{t_1}, \dots, a_{t_K})$. In this framework,
 182 the goal is to train a policy π to predict the key-frame action a_{t_k} at the closest next key-frame of
 183 timestep t_k given an observation o_t and a task description L_i :

$$\pi(o_t, L_i) \rightarrow a_{t_k} \text{ for } t_{k-1} \leq t < t_k. \quad (1)$$

186 The predicted actions are executed by a motion planner, which moves the robot to the desired state,
 187 generating thus the intermediate actions in a trajectories. In coarse-to-fine policies, the 3D position
 188 p_{t_k} output by the coarse branch for the next key-frame is typically used as the 3D keypoint to zoom
 189 into the observation for the action predictor.

190 In RVT2, multi-view RGB-D images are first aggregated into a point cloud, which is then projected
 191 into three canonical views: front, left and top. These three views are orthogonal to each other,
 192 which allows a mapping between pixel positions in these views and a 3D position in the scene.
 193 Each pixel in the projected images contains 3-channel RGB values, 1-channel depth value and its
 194 corresponding 3D position in the global coordinate. In the coarse branch, the projected images are
 195 tokenized using convolutional layers while the task description and robot states (e.g., gripper status)
 196 are encoded by a pre-trained language encoder and a trainable Multi-Layer-Perceptron respectively.
 197 All these tokenized features are fused via Multi-View Transformer (Goyal et al., 2023). The image
 198 tokens in the output of the transformer are then processed by upsampling layers to predict heatmaps,
 199 from which a 3D keypoint is extracted. The keypoint from the coarse branch is used to zoom in
 200 and crop the point cloud while the cropped region is again projected into the canonical views. The
 201 refined observations along with the same task description are processed by the fine-grained branch,
 202 implemented as another multi-view transformer with different weights, to predict the final actions.
 203 While RVT2 achieves strong sample efficiency and enables precise manipulation via projections to
 204 canonical views and its coarse-to-fine architecture, it is trained from scratch and therefore does not
 205 leverage recent pretrained large models. In addition, its architecture design does not fully exploit
 206 common skills among tasks. As a result, it suffers from deficient generalization to visual changes,
 207 object variations, and novel tasks.

208

4 METHOD

210 Our hierarchical policy consists of a coarse task planner and a fine-grained action predictor, as
 211 shown in Figure 2. To promote compositional generalization, we first decompose tasks into step-
 212 wise language instructions, each describing the motion of the robot between two consecutive key-
 213 frames. This enables the coarse task planner to perform language-guided planning while allowing
 214 the fine-grained action predictor to learn and reuse common skills across tasks. Moreover, we adapt
 215 a pre-trained VLM to 3D keypoint prediction in the coarse task planner, by finetuning it with a
 sequential reasoning procedure. [The VLM predicts the pixel position in each view and we follow](#)

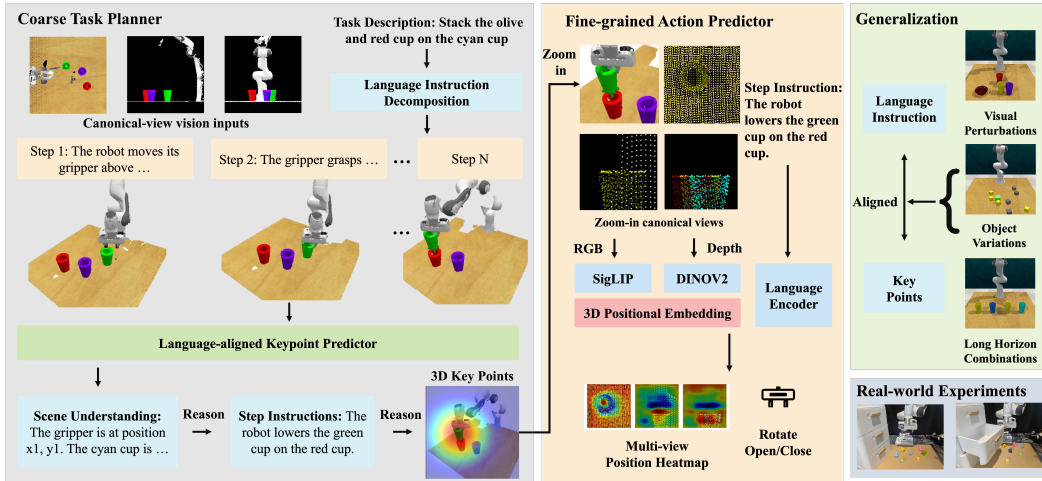


Figure 2: **Overview of CLAP.** We propose a novel coarse-to-fine 3D manipulation policy, comprising of a coarse task planner and a fine-grained action predictor. The coarse task planner reasons about the task plans and the positions of task-related objects to generate language-aligned 3D keypoints. The fine-grained action predictor fuses the corresponding step instruction with a 3D-aware visual representation from refined observations to predict the final action.

the prior work (Goyal et al., 2024) to map them to a 3D position. The pretrained VLM is trained to first reason about the positions of task-related objects, then generate a step instruction and finally predict the corresponding 3D keypoints. To enable zero-shot generalization ability to novel objects, we add an auxiliary task of 3D object detection by augmenting the training data with additional object positions dataset. Finally, in contrast to RVT2, the coarse and fined-grained branches are implemented with a different architecture, since they play different roles. Thus, for the latter, we utilize specialized pre-trained visual foundation models to construct a 3D-aware representation. The design choices of both the coarse task planner and the fine-grained action predictor are detailed in the following sections.

4.1 COARSE TASK PLANNER

Prior coarse-to-fine policies condition all actions within a trajectory on a single high-level task description, limiting compositional generalization. To address this, we leverage a pre-trained VLM, denoted f_θ , to decompose a high-level task description L into step-wise language instructions $\mathcal{L} = (\ell_1, \dots, \ell_k, \dots, \ell_K)$, which naturally align with the key-frame based trajectory segmentation. Each trajectory segment $(o_{t_{k-1}+1}, a_{t_{k-1}+1}, \dots, o_{t_k}, a_{t_k})$ and key-frame action a_{t_k} have a corresponding step instruction ℓ_k describing the motion of the robot within the segment. For example, the task "open the top drawer" is decomposed into following step instructions: ℓ_1 : "The robot arm lowers itself to align with the handle of the top drawer", ℓ_2 : "The robot arm grasps the top drawer's handle firmly", and ℓ_3 : "The robot pulls the handle back, smoothly opening the top drawer".

In addition to task decomposition done at the beginning, at every execution timestep, the VLM f_θ is also exploited to predict both the step instruction ℓ_{t_k} (used as a novel input of the action predictor) and its language-aligned 3D keypoint p_{t_k} (for cropping a region of interest, as usually done in coarse-to-fine policies). We discuss next how this prediction can be realized effectively.

Task decomposition enables reasoning about task plans before predicting actions. However, directly training the model f_θ to simultaneously generate a task plan \mathcal{L} and predict step instruction ℓ_{t_k} and 3D keypoint p_{t_k} , given as inputs multi-view images obtained from observation $o_{t_{k-1}}$ and a high-level task description L , (i.e., $f_\theta(o_{t_{k-1}}, L) \rightarrow (\mathcal{L}, \ell_{t_k}, p_{t_k})$), does not ensure generalization to novel instructions. Previous studies (Kim et al., 2024; Intelligence et al., 2025; Zhao et al., 2025; Gao et al., 2025) indicate that VLAs exhibit a strong bias towards visual inputs, due to the richer information embedded in the visual inputs. This reliance often causes failures to follow novel language instructions. Under our data-scarce training setting, this issue is intensified by the limited

270 diversity of language instructions. To address this issue, we propose decoupling task planning from
 271 keypoint prediction via a two-round inference protocol. First, a purely textual query generates a
 272 language plan, the sequence of all step instructions \mathcal{L} . Second, the visual inputs augmented with
 273 this plan are used to predict the corresponding step instruction and keypoint:

$$f_{\theta}(L_i) \rightarrow \mathcal{L}, f_{\theta}(o_{t_{k-1}}, \mathcal{L}) \rightarrow (\ell_{t_k}, p_{t_k}). \quad (2)$$

276 This approach not only mitigates visual bias but also enables training with an auxiliary dataset of
 277 language plans, which serves as a manual to enhance compositional task reasoning.

278 For a plan \mathcal{L} corresponding to a task description L , directly fine-tuning a VLM to predict both the
 279 step instruction ℓ_{t_k} and its language-aligned 3D keypoint p_{t_k} reveals to be insufficient due to the
 280 inadequate alignment of the visual-textual embeddings of the VLM for this 3D keypoint predic-
 281 tion. Instead, inspired by Chain-of-Thought reasoning (Mu et al., 2023; Zawalski et al., 2024; Zhao
 282 et al., 2025) for robotics, we design a reasoning process by training our model to first reason about
 283 the pixel positions of task-related objects, then generate a step instruction and finally predict the
 284 corresponding keypoint, changing the second step of Equation (2) to:

$$f_{\theta}(o_{t_{k-1}}, \mathcal{L}) \rightarrow (p_{obj}, \ell_{t_k}, p_{t_k}), \quad (3)$$

285 where p_{obj} are the 3D positions of the task-related objects.

286 We further observe that for long-horizon, especially repetitive tasks (e.g., "stack several blocks"),
 287 only providing the entire task plan whether as input or output can degrade the performance. This
 288 often causes the model to generate repetitive sequences until reaching the output length limit or to
 289 struggle in determining the next step from an excessively long plan. To mitigate this, we introduce
 290 two ideas. First, we provide to the VLM an additional input: the step instruction predicted in the last
 291 timestep, which serves as a short-term memory cue to contextualize the current situation. Moreover,
 292 we decompose the plan into sub-tasks, i.e., $\mathcal{L} = (\mathcal{L}_1 = (\ell_1, \ell_2, \dots, \ell_n), \mathcal{L}_2 = (\ell_{n+1}, \ell_{n+2}, \dots), \dots)$.
 293 For instance, "stack the blue and yellow cup on the red cup" is decomposed into two sequential
 294 sub-tasks: \mathcal{L}_1 "stack the blue on the red cup" followed by \mathcal{L}_2 "stack the yellow cup on the red cup".
 295 The model is trained to generate only the task plan of current sub-task, preventing repetition and
 296 improving focus:

$$f_{\theta}(L, \hat{\ell}) \rightarrow \mathcal{L}_m, f_{\theta}(o_{t_{k-1}}, \mathcal{L}_m, \hat{\ell}) \rightarrow (p_{obj}, \ell_{t_k}, p_{t_k}), \quad (4)$$

297 where $\hat{\ell}$ is the step instruction predicted in the last timestep and \mathcal{L}_m is the language plan of the m^{th}
 298 sub-task. At the beginning of a trajectory, where no previous timestep exists, $\hat{\ell}$ is defined as "the
 299 robot is currently at the initial state" to indicate the initial state.

300 To further enhance the generalization ability of the coarse task planner to object variations, we
 301 include an auxiliary task of predicting the object positions. We randomly initialize diverse
 302 environments and record the RGB-D images of the scene along with the 3D positions of the objects.
 303 Following the same pre-processing, both the RGB-D images and the 3D positions of the objects are
 304 projected into canonical views. The projected multi-view images and pixel coordinates of the object
 305 positions in each view are used to construct an object position dataset. This dataset is then utilized
 306 to co-train the VLM, reinforcing its spatial understanding and improving zero-shot generalization to
 307 object variations.

312 4.2 FINE-GRAINED ACTION PREDICTOR

313 The fine-grained action predictor uses a predicted step instruction ℓ_{t_k} , instead of the original high-
 314 level task description L , enabling more precise and generalizable skill learning. Considering the
 315 significant domain shift between the images focused around predicted p_{t_k} from those used to pre-
 316 train standard VLMs, we decide to employ instead pre-trained specialized encoders to process these
 317 inputs. Our feature encoding pipeline consists of three stages to construct a unified 3D-aware and
 318 language-aligned representation. First, RGB images and step instructions are processed through
 319 vision-language encoders to establish semantic alignment between visual and textual inputs. Second,
 320 depth images are encoded separately to extract explicit geometric structure. Finally, we generate a
 321 3D position embedding from pixel-wise 3D coordinates to incorporate spatial awareness. These
 322 components are combined to form a 3D-aware, language-aligned representation for downstream
 323 fine-grained action prediction, following the architecture of prior work (Goyal et al., 2024).

Models	Avg.	Success \uparrow	L1	L2	L3	L4
HiveFormer (Guhur et al., 2023)	30.4	60.3 ± 1.5	26.1 ± 1.4	35.1 ± 1.7	0.0 ± 0.0	
PolarNet (Chen et al., 2023)	38.4	77.7 ± 0.9	37.1 ± 1.4	38.5 ± 1.7	0.1 ± 0.2	
3D Diffuser Actor (Ke et al., 2024)	44.0	91.9 ± 0.8	43.4 ± 2.8	37.0 ± 2.2	0.0 ± 0.0	
RVT2 (Goyal et al., 2024)	44.0	89.1 ± 0.8	51.0 ± 2.3	36.0 ± 2.2	0.0 ± 0.0	
3D-LOTUS (Garcia et al., 2025)	45.7	94.3 ± 1.4	49.9 ± 2.2	38.1 ± 1.1	0.3 ± 0.3	
3D-LOTUS++ (Garcia et al., 2025)	48.0	68.7 ± 0.6	64.5 ± 0.9	41.5 ± 1.8	17.4 ± 0.4	
BridgeVLA (Li et al., 2025b)	50.0	91.1 ± 1.1	65.0 ± 1.3	43.8 ± 1.2	0.0 ± 0.0	
CLAP (Proposed)	62.0	83.9 ± 0.3	83.2 ± 1.9	49.6 ± 2.1	31.4 ± 0.6	

Table 1: **Multi-Task Performance on GemBench.** Here are the average success rates of 4 levels of evaluation tasks from Gembench. Except CLAP, we use the results reported in BridgeVLA.

5 EXPERIMENTS

We now present the experimental settings and results in simulation and real-world experiments.

5.1 SIMULATION RESULTS

Experimental Set-up Our method is evaluated on GemBench (Garcia et al., 2025), a benchmark specifically designed for evaluating the generalization ability of a policy. A dataset containing 100 demonstrations per task along with a task description per trajectory is prepared for training. This training set contains 16 tasks with 31 variations. Within a trajectory, 4 cameras are placed at the front, left shoulder, right shoulder and wrist to collect RGB-D images as the observations. The resolution of the original RGB-D images is 256x256 while the resolution of the projected images is 224x224. Instead of evaluating on in-distribution tasks and variations, GemBench designs an evaluation set containing 4 levels of tasks, where different elements are varied:

- **Placements (L1):** same 16 tasks (31 variations) as in training set, but with novel object placements.
- **Rigid Objects (L2):** 15 novel tasks (28 variations) with newly-colored or -shaped rigid objects.
- **Articulated Objects (L3):** 18 novel tasks (21 variations) with appearance or object variation.
- **Long-horizon Tasks (L4):** 6 novel long-horizon tasks (12 variations).

The specific configuration for tasks used for training and evaluation in GemBench are listed in Appendix A.1. We explain in detail how we create the language plan dataset and object position dataset in Appendix A.2. Following the evaluation setting in GemBench (Garcia et al., 2025), all trained models are evaluated with 20 episodes per task variation per seed, and 5 different seeds are used.

In our method, we finetune Qwen 2.5 VL-3B (Bai et al., 2025) as the coarse task planner. It is LoRA fine-tuned (Hu et al., 2022) with the object keypoint dataset, language plans, and robot trajectories. We use SigLIP (Zhai et al., 2023) to extract features from the RGB images and step instructions, leveraging its language-aligned representations. For depth images, we use DINOv2 (Oquab et al., 2023), which excels at capturing geometric structures like edges and contours. We further enhance these features by using the 3D coordinate of each pixel to construct a 3D position embedding. The hyperparameters, such as batch size and learning rate used in training are listed in Appendix A.3.

To construct the fine-tuning dataset from robot trajectories, we design a sampling strategy to choose samples from the trajectories. Apart from key-frame pairs of observation and action $(o_{t_k}, a_{t_{k+1}})$, RVT2 augments the training data by sampling observations every n frames (e.g., every 10 frames). However, this results in an uneven number of samples per trajectory segment, due to the varying length of each segment. We initially attempted to sample observations within a window $(o_{t_k-m}, \dots, o_{t_k}, \dots o_{t_k+m})$ around the time step t_k of the k^{th} key-frame. However, observations at time steps before a key-frame and after a key-frame are visually similar while corresponding to distinct actions. For example, o_{t_k-1} and o_{t_k+1} are similar while their corresponding keypoints are the gripper positions at t_k and t_{k+1} respectively. Using all observations around the key-frames to fine-tune the VLM risks confusing it. Finally, we choose to use observations $(o_{t_k}, \dots o_{t_k+m})$ at the time steps immediately following each key-frame. We empirically choose m as 5 in all experiments.

Main Results The evaluation results on GemBench are summarized in Table 1, reporting the average success rate for tasks at each generalization level. The detailed success rate for each task are

378	Exp	Language	Plan	Object	Keypoints	Last	Reason	Reason	Pretrained	Level	Level	Level	Level	Avg.
379	ID	Data		Data		Step	Plan	Objects	Encoder	1	2	3	4	Succ.
380	1	X		X		X	X	X	✓	86.9	68.2	36.4	0.4	48.0
381	2	X		X		X	X	✓	✓	81.8	74.8	39.0	0	48.9
382	3	✓		X		✓	✓	X	✓	83.4	66.1	41.9	2.0	48.3
383	4	✓		X		✓	✓	✓	✓	84.8	81.4	43.8	30.4	60.1
384	5	✓		✓		✓	✓	✓	X	82.4	79.1	44.5	25	57.8
385	6	✓		✓		✓	✓	✓	✓	83.8	83.2	49.6	31.4	62.0

Table 2: **Ablation study of CLAP on GemBench.** Here are the average success rates of 4 levels of evaluation tasks from Gembench under different training settings.

recorded in Appendix A.4. The experimental results demonstrate the strong generalization ability of our method to novel tasks and object variations, as indicated by the performance gain on Level-2, Level-3, and Level-4 tasks. Our method achieves an overall success rate 12% higher than prior state-of-the-art method (Li et al., 2025b). Notably, this improvement is obtained using only 20 trajectories per task variation for training, significantly fewer than the 100 trajectories used by other baselines. Furthermore, our design leads to substantial performance gain on the most challenging Level-4 tasks, where several baselines methods fail consistently. [We also include an experiments on the effects of using different number of trajectories in Appendix A.5.](#)

Ablation We further experimentally validate the design choice for both coarse task planner and fine-grained action predictor on GemBench. The configurations are detailed below and corresponding results are presented in Table 2. [A specific ablation on the inputs of the fine-grained action predictor is include in Appendix A.5.](#)

1) **Base** In the base version (corresponding to Exp ID 1), the coarse task planner is trained with only the robot trajectories to predict step instruction and the corresponding keypoints. We use this version as a baseline to ablate our method.

2) **Object Reasoning** To adapt the pre-trained VLM for 3D keypoint prediction, we introduce a structured reasoning procedure where the model first localizes task-relevant objects before predicting the step instruction and its corresponding keypoint. We evaluate the efficacy of this object position reasoning in Exp ID 2. A comparison with the base model (Exp ID 1) reveals a performance improvement on Level-2 and Level-3 tasks, indicating enhanced generalization to object variations.

3) **Language Plan Reasoning** The proposed task decomposition enables a two-round conversation, where a language plan is first generated through textual reasoning, followed by keypoint prediction. This approach also permits the inclusion of additional language plans during training to enhance compositional generalization. Compared to the base model (Exp ID 1), this version shows improvements on Level 3 and Level 4 tasks, demonstrating stronger generalization to novel task variations.

4) **Include Previous Step Instruction** Previous step instruction is included in the input as a short-term memory to help contextualize the current status. This design yields performance gains across Levels 2, 3, and 4, with particularly notable improvements on long-horizon tasks in Level 4.

5) **CLAP w/o Pre-trained Encoder** An ablation study (comparing Exp ID 5 and Exp ID 6) on the coarse planner confirms that incorporating the 3D-aware representation contributes to performance gains at all generalization levels.

6) **CLAP** Our method integrates all components mentioned above. A comparison between Exp ID 4 and ours can further validate the performance gain from adding the object position dataset.

5.2 REAL-WORLD EXPERIMENTS

Experimental Setting We keep the training settings the same as in the simulation and list key modifications here. In the real-world experiments, we use a single camera (Intel RealSense D435i) to collect RGB-D images of size 640x360. 10 trajectories are collected per task to cover all variations of each task. The hyperparameters used for training the models are listed in Appendix A.3. The training tasks, illustrated in Figure 3, are listed below. 1) Place shape in shape sorter: insert objects into a box with 3 variations on the object shape. 2) Put block in cup: put a colored block in a same-

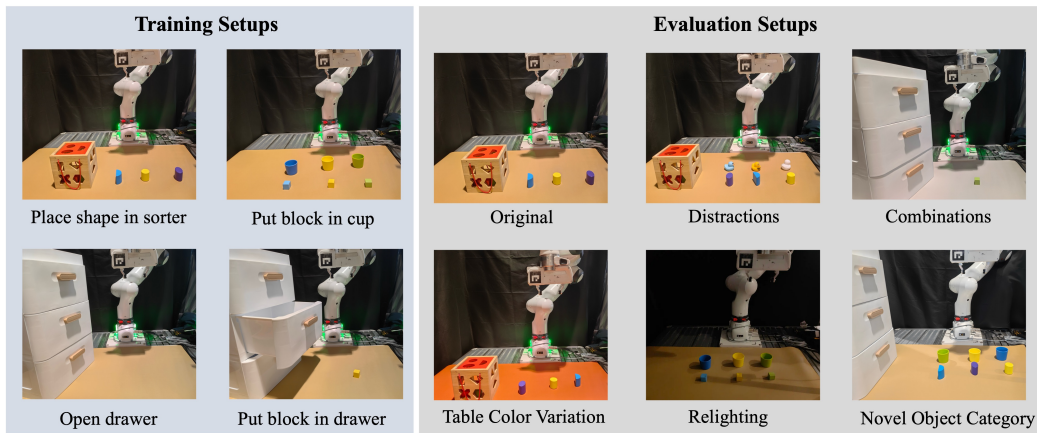


Figure 3: **Overview of the tasks in real-world experiments.** There are four training tasks: put shape in shape sorter, put block in cup, open drawer, put block in drawer. We evaluate the same tasks under different visual perturbations and novel tasks designed based on the training tasks.

	No Variation		Table Color		Distracted Objects		Light Strength		Average Succ.	
	RVT2	CLAP	RVT2	CLAP	RVT2	CLAP	RVT2	CLAP	RVT2	CLAP
place shape in shape sorter	60%	60%	35%	50%	30%	40%	20%	50%	36.2%	50%
put block in cup with same color	40%	100%	20%	70%	20%	80%	20%	80%	25%	82.5%
open drawer	100%	100%	85%	95%	100%	100%	0%	100%	71.2%	98.7%
put block in open drawer	40%	90%	25%	90%	20%	70%	0%	90%	21.2%	85%
put block in cup with different color	20%	100%	15%	70%	0%	70%	10%	80%	11.2%	80%
put shape in open drawer	30%	80%	20%	65%	10%	70%	0%	80%	15%	73.7%
put shape in cup	0%	80%	0%	70%	0%	60%	0%	70%	0%	70%
put block in close drawer	0%	90%	0%	75%	0%	70%	0%	80%	0%	78.7%
average success rate	36.2%	87.5%	25%	73.1%	22.5%	70%	6.2%	78.7%	22.5%	77.3%

Table 3: **Real-world Performance.** Here are the average success rate under different generalization settings for real-world experiments.

colored cup with 3 variations on colors. 3) Open drawer: open a drawer with 3 variations on the handles. 4) Put a block in drawer: put a colored block in an open drawer with 3 variations on colors.

We assess the generalization ability of CLAP along two key dimensions (see Appendix A.6 for an overview of these evaluation tasks):

- 1) **Visual Perturbations:** The model is tested on the tasks same as the training tasks but with the following conditions: different table colors, introducing distracting objects and altered backgrounds.
- 2) **Task/Object Variations:** Generalization is evaluated through: i) Object substitution (e.g., placing a "shape" object into a cup), and ii) Skill composition (e.g., combining "open drawer" and "place block" into a single, sequential task).

Results The results of evaluating the trained models in real-world experiments are summarized in Table 3. Our method achieves a strong generalization ability to novel tasks and object variations, trained with only 10 demonstrations per task. CLAP achieves 54.8% higher average success rates compared to RVT2 on the evaluation tasks.

6 CONCLUSIONS

We propose a novel coarse-to-fine 3D manipulation policy, where tasks are decomposed and pre-trained models are leveraged in the hierarchical architecture. Our method demonstrates strong generalization capabilities while maintaining the sample efficiency inherent to coarse-to-fine approaches. Although leveraging pre-trained models for robotics tasks is common, their effective adaptation for generalizable and precise is still under-explored. We hope this work inspires further research into building highly generalizable and sample-efficient 3D manipulation policies. Our method has two

486 key limitations. First, key-frame based imitation learning is suitable for structured tasks that can
 487 be easily decomposed into discrete steps. Unstructured tasks, such as wiping a desk, where key-
 488 frames are difficult to define, present a significant challenge. Moreover, the current framework lacks
 489 a robust error-correction mechanism. An incorrect action prediction at any step might lead to task
 490 failure. A promising future direction is to integrate a self-correction module to enhance robustness.
 491

492 **LLM Usage** We used Deepseek (AI, 2024) and ChatGPT (OpenAI, 2024) for grammar check and
 493 related work retrieval. The authors have reviewed the content generated by the LLM.
 494

495 **Ethics Statement** We adhere to the ICLR Code of Ethics and take full responsibility for the final
 496 content.
 497

498 **Reproducibility Statement** To ensure reproducibility, we provide a comprehensive description of
 499 our method and experimental setup in the Section 4 and the Section 5, document all hyperparameters
 500 in the appendix Table 6, and will release our code publicly upon acceptance.
 501

502 REFERENCES

504 DeepSeek AI. Deepseek-v3. <https://deepseek.com>, 2024. Model and technical details
 505 available at <https://github.com/deepseek-ai>.
 506

507 Shuai Bai, Keqin Chen, Xuejing Liu, Jialin Wang, Wenbin Ge, Sibo Song, Kai Dang, Peng Wang,
 508 Shijie Wang, Jun Tang, Humen Zhong, Yuanzhi Zhu, Mingkun Yang, Zhaohai Li, Jianqiang Wan,
 509 Pengfei Wang, Wei Ding, Zheren Fu, Yiheng Xu, Jiabo Ye, Xi Zhang, Tianbao Xie, Zesen Cheng,
 510 Hang Zhang, Zhibo Yang, Haiyang Xu, and Junyang Lin. Qwen2.5-v1 technical report. *arXiv
 511 preprint arXiv:2502.13923*, 2025.

512 Lucas Beyer, Andreas Steiner, André Susano Pinto, Alexander Kolesnikov, Xiao Wang, Daniel Salz,
 513 Maxim Neumann, Ibrahim Alabdulmohsin, Michael Tschannen, Emanuele Bugliarello, Thomas
 514 Unterthiner, Daniel Keysers, Skanda Koppula, Fangyu Liu, Adam Grycner, Alexey Gritsenko,
 515 Neil Houlsby, Manoj Kumar, Keran Rong, Julian Eisenschlos, Rishabh Kabra, Matthias Bauer,
 516 Matko Bošnjak, Xi Chen, Matthias Minderer, Paul Voigtlaender, Ioana Bica, Ivana Balazevic,
 517 Joan Puigcerver, Pinelopi Papalampidi, Olivier Henaff, Xi Xiong, Radu Soricut, Jeremiah Harm-
 518 sen, and Xiaohua Zhai. Paligemma: A versatile 3b vlm for transfer, 2024. URL <https://arxiv.org/abs/2407.07726>.
 519

520 Anthony Brohan, Noah Brown, Justice Carbajal, Yevgen Chebotar, Xi Chen, Krzysztof Choro-
 521 manski, Tianli Ding, Danny Driess, Avinava Dubey, Chelsea Finn, Pete Florence, Chuyuan Fu,
 522 Montse Gonzalez Arenas, Keerthana Gopalakrishnan, Kehang Han, Karol Hausman, Alex Her-
 523 zog, Jasmine Hsu, Brian Ichter, Alex Irpan, Nikhil Joshi, Ryan Julian, Dmitry Kalashnikov,
 524 Yuheng Kuang, Isabel Leal, Lisa Lee, Tsang-Wei Edward Lee, Sergey Levine, Yao Lu, Hen-
 525 ryk Michalewski, Igor Mordatch, Karl Pertsch, Kanishka Rao, Krista Reymann, Michael Ryoo,
 526 Grecia Salazar, Pannag Sanketi, Pierre Sermanet, Jaspia Singh, Anikait Singh, Radu Soricut,
 527 Huong Tran, Vincent Vanhoucke, Quan Vuong, Ayzaan Wahid, Stefan Welker, Paul Wohlhart,
 528 Jialin Wu, Fei Xia, Ted Xiao, Peng Xu, Sichun Xu, Tianhe Yu, and Brianna Zitkovich. Rt-
 529 2: Vision-language-action models transfer web knowledge to robotic control. In *arXiv preprint
 530 arXiv:2307.15818*, 2023.

531 Chilam Cheang, Sijin Chen, Zhongren Cui, Yingdong Hu, Liqun Huang, Tao Kong, Hang Li, Yifeng
 532 Li, Yuxiao Liu, Xiao Ma, Hao Niu, Wenxuan Ou, Wanli Peng, Zeyu Ren, Haixin Shi, Jiawen Tian,
 533 Hongtao Wu, Xin Xiao, Yuyang Xiao, Jiafeng Xu, and Yichu Yang. Gr-3 technical report, 2025.
 534 URL <https://arxiv.org/abs/2507.15493>.
 535

536 Shizhe Chen, Ricardo Garcia Pinel, Cordelia Schmid, and Ivan Laptev. Polarnet: 3d point
 537 clouds for language-guided robotic manipulation. In Jie Tan, Marc Toussaint, and Kourosh
 538 Darvish (eds.), *Proceedings of The 7th Conference on Robot Learning*, volume 229 of *Pro-
 539 ceedings of Machine Learning Research*, pp. 1761–1781. PMLR, 06–09 Nov 2023. URL
<https://proceedings.mlr.press/v229/chen23b.html>.

540 Yangtao Chen, Zixuan Chen, Junhui Yin, Jing Huo, Pinzhuo Tian, Jieqi Shi, and Yang
 541 Gao. Gravmad: Grounded spatial value maps guided action diffusion for general-
 542 ized 3d manipulation. In Y. Yue, A. Garg, N. Peng, F. Sha, and R. Yu (eds.), *Int-
 543 ernational Conference on Representation Learning*, volume 2025, pp. 102042–102074,
 544 2025a. URL https://proceedings.iclr.cc/paper_files/paper/2025/file/fce176458ff542940fa3ed16e6f9c852-Paper-Conference.pdf.

545

546 Zixuan Chen, Junhui Yin, Yangtao Chen, Jing Huo, Pinzhuo Tian, Jieqi Shi, Yiwen Hou, Yinchuan
 547 Li, and Yang Gao. Deco: Task decomposition and skill composition for zero-shot generalization
 548 in long-horizon 3d manipulation, 2025b. URL <https://arxiv.org/abs/2505.00527>.

549

550 Danny Driess, Fei Xia, Mehdi S. M. Sajjadi, Corey Lynch, Aakanksha Chowdhery, Brian Ichter,
 551 Ayzaan Wahid, Jonathan Tompson, Quan Vuong, Tianhe Yu, Wenlong Huang, Yevgen Chebotar,
 552 Pierre Sermanet, Daniel Duckworth, Sergey Levine, Vincent Vanhoucke, Karol Hausman, Marc
 553 Toussaint, Klaus Greff, Andy Zeng, Igor Mordatch, and Pete Florence. PaLM-e: An embodied
 554 multimodal language model. In Andreas Krause, Emma Brunskill, Kyunghyun Cho, Barbara
 555 Engelhardt, Sivan Sabato, and Jonathan Scarlett (eds.), *Proceedings of the 40th International
 556 Conference on Machine Learning*, volume 202 of *Proceedings of Machine Learning Research*, pp.
 557 8469–8488. PMLR, 23–29 Jul 2023. URL <https://proceedings.mlr.press/v202/driess23a.html>.

558

559 Haoquan Fang, Markus Grotz, Wilbert Pumacay, Yi Ru Wang, Dieter Fox, Ranjay Krishna, and
 560 Jiafei Duan. Sam2act: Integrating visual foundation model with a memory architecture for robotic
 561 manipulation. In *Proceedings of the 42nd International Conference on Machine Learning*, 2025.

562

563 Chongkai Gao, Zixuan Liu, Zhenghao Chi, Junshan Huang, Xin Fei, Yiwen Hou, Yuxuan Zhang,
 564 Yudi Lin, Zhirui Fang, Zeyu Jiang, and Lin Shao. Vla-os: Structuring and dissecting planning rep-
 565 resentations and paradigms in vision-language-action models. *arXiv preprint arXiv:2506.17561*,
 566 2025. URL <https://arxiv.org/abs/2506.17561>.

567

568 Ricardo Garcia, Shizhe Chen, and Cordelia Schmid. Towards generalizable vision-language robotic
 569 manipulation: A benchmark and llm-guided 3d policy. In *International Conference on Robotics
 570 and Automation (ICRA)*, 2025.

571

572 Theophile Gervet, Zhou Xian, Nikolaos Gkanatsios, and Katerina Fragkiadaki. Act3d: 3d fea-
 573 ture field transformers for multi-task robotic manipulation. In Jie Tan, Marc Toussaint, and
 574 Kourosh Darvish (eds.), *Proceedings of The 7th Conference on Robot Learning*, volume 229
 575 of *Proceedings of Machine Learning Research*, pp. 3949–3965. PMLR, 06–09 Nov 2023. URL
<https://proceedings.mlr.press/v229/gervet23a.html>.

576

577 Ankit Goyal, Jie Xu, Yijie Guo, Valts Blukis, Yu-Wei Chao, and Dieter Fox. Rvt: Robotic view
 578 transformer for 3d object manipulation. In Jie Tan, Marc Toussaint, and Kourosh Darvish (eds.),
 579 *Proceedings of The 7th Conference on Robot Learning*, volume 229 of *Proceedings of Machine
 580 Learning Research*, pp. 694–710. PMLR, 06–09 Nov 2023. URL <https://proceedings.mlr.press/v229/goyal23a.html>.

581

582 Ankit Goyal, Valts Blukis, Jie Xu, Yijie Guo, Yu-Wei Chao, and Dieter Fox. Rvt2: Learning precise
 583 manipulation from few demonstrations. *RSS*, 2024.

584

585 Marcus Gualtieri and Robert Platt. Learning 6-dof grasping and pick-place using attention fo-
 586 cus. In Aude Billard, Anca Dragan, Jan Peters, and Jun Morimoto (eds.), *Proceedings of The
 587 2nd Conference on Robot Learning*, volume 87 of *Proceedings of Machine Learning Research*,
 588 pp. 477–486. PMLR, 29–31 Oct 2018. URL <https://proceedings.mlr.press/v87/gualtieri18a.html>.

589

590 Marcus Gualtieri and Robert Platt. Learning manipulation skills via hierarchical spatial attention.
 591 *IEEE Transactions on Robotics*, 36(4):1067–1078, August 2020. ISSN 1941-0468. doi: 10.1109/
 592 tro.2020.2974093. URL <http://dx.doi.org/10.1109/TRO.2020.2974093>.

593

Pierre-Louis Guhur, Shizhe Chen, Ricardo Garcia Pinel, Makarand Tapaswi, Ivan Laptev, and
 594 Cordelia Schmid. Instruction-driven history-aware policies for robotic manipulations. In Karen

594 Liu, Dana Kulic, and Jeff Ichniowski (eds.), *Proceedings of The 6th Conference on Robot Learning*,
 595 volume 205 of *Proceedings of Machine Learning Research*, pp. 175–187. PMLR, 14–18 Dec
 596 2023. URL <https://proceedings.mlr.press/v205/guhur23a.html>.

597 Edward J Hu, yelong shen, Phillip Wallis, Zeyuan Allen-Zhu, Yuanzhi Li, Shean Wang, Lu Wang,
 598 and Weizhu Chen. LoRA: Low-rank adaptation of large language models. In *International Con-
 599 ference on Learning Representations*, 2022. URL [https://openreview.net/forum?
 600 id=nZeVKeeFYf9](https://openreview.net/forum?id=nZeVKeeFYf9).

601 Physical Intelligence, Kevin Black, Noah Brown, James Darpinian, Karan Dhabalia, Danny Driess,
 602 Adnan Esmail, Michael Equi, Chelsea Finn, Niccolo Fusai, Manuel Y. Galliker, Dibya Ghosh,
 603 Lachy Groom, Karol Hausman, Brian Ichter, Szymon Jakubczak, Tim Jones, Liyiming Ke, Devin
 604 LeBlanc, Sergey Levine, Adrian Li-Bell, Mohith Mothukuri, Suraj Nair, Karl Pertsch, Allen Z.
 605 Ren, Lucy Xiaoyang Shi, Laura Smith, Jost Tobias Springenberg, Kyle Stachowicz, James Tanner,
 606 Quan Vuong, Homer Walke, Anna Walling, Haohuan Wang, Lili Yu, and Ury Zhilinsky. $\pi_{0.5}$: a
 607 vision-language-action model with open-world generalization, 2025. URL <https://arxiv.org/abs/2504.16054>.

608

609 Stephen James, Kentaro Wada, Tristan Laidlow, and Andrew J. Davison. Coarse-to-fine q-attention:
 610 Efficient learning for visual robotic manipulation via discretisation. In *2022 IEEE/CVF Con-
 611 ference on Computer Vision and Pattern Recognition (CVPR)*, pp. 13729–13738, 2022. doi:
 612 10.1109/CVPR52688.2022.01337.

613

614 Yueru Jia, Jiaming Liu, Sixiang Chen, Chenyang Gu, Zhilve Wang, Longzan Luo, Xiaoqi Li, Peng-
 615 wei Wang, Zhongyuan Wang, Renrui Zhang, and Shanghang Zhang. Lift3d policy: Lifting 2d
 616 foundation models for robust 3d robotic manipulation. In *Proceedings of the IEEE/CVF Confer-
 617 ence on Computer Vision and Pattern Recognition (CVPR)*, pp. 17347–17358, June 2025.

618

619 Edward Johns. Coarse-to-fine imitation learning: Robot manipulation from a single demonstration.
 620 In *IEEE International Conference on Robotics and Automation (ICRA)*, 2021.

621

622 Tsung-Wei Ke, Nikolaos Gkanatsios, and Katerina Fragkiadaki. 3d diffuser actor: Policy diffusion
 623 with 3d scene representations, 2024. URL <https://arxiv.org/abs/2402.10885>.

624

625 Moo Jin Kim, Karl Pertsch, Siddharth Karamcheti, Ted Xiao, Ashwin Balakrishna, Suraj Nair,
 626 Rafael Rafailov, Ethan Foster, Grace Lam, Pannag Sanketi, Quan Vuong, Thomas Kollar, Ben-
 627 jamin Burchfiel, Russ Tedrake, Dorsa Sadigh, Sergey Levine, Percy Liang, and Chelsea Finn.
 628 Openvla: An open-source vision-language-action model. *arXiv preprint arXiv:2406.09246*, 2024.

629

630 Chengmeng Li, Junjie Wen, Yan Peng, Yixin Peng, Feifei Feng, and Yichen Zhu. Pointvla: Injecting
 631 the 3d world into vision-language-action models, 2025a. URL <https://arxiv.org/abs/2503.07511>.

632

633 Peiyan Li, Yixiang Chen, Hongtao Wu, Xiao Ma, Xiangnan Wu, Yan Huang, Liang Wang, Tao
 634 Kong, and Tieniu Tan. Bridgevla: Input-output alignment for efficient 3d manipulation learning
 635 with vision-language models, 2025b. URL <https://arxiv.org/abs/2506.07961>.

636

637 Qixiu Li, Yaobo Liang, Zeyu Wang, Lin Luo, Xi Chen, Mozheng Liao, Fangyun Wei, Yu Deng,
 638 Sicheng Xu, Yizhong Zhang, et al. Cogact: A foundational vision-language-action model for
 639 synergizing cognition and action in robotic manipulation. *arXiv preprint arXiv:2411.19650*, 2024.

640

641 Suhan Ling, Yian Wang, Ruihai Wu, Shiguang Wu, Yuzheng Zhuang, Tianyi Xu, Yu Li, Chang Liu,
 642 and Hao Dong. Articulated object manipulation with coarse-to-fine affordance for mitigating the
 643 effect of point cloud noise. In *2024 IEEE International Conference on Robotics and Automation
 644 (ICRA)*, pp. 10895–10901, 2024. doi: 10.1109/ICRA57147.2024.10610593.

645

646 Songming Liu, Lingxuan Wu, Bangguo Li, Hengkai Tan, Huayu Chen, Zhengyi Wang, Ke Xu, Hang
 647 Su, and Jun Zhu. Rdt-1b: a diffusion foundation model for bimanual manipulation. *International
 648 Conference on Learning Representations (ICLR)*, 2024.

649

650 Yangjun Liu, Sheng Liu, Binghan Chen, Zhi-Xin Yang, and Sheng Xu. Fusion-perception-to-action
 651 transformer: Enhancing robotic manipulation with 3-d visual fusion attention and proprioception.
 652 *IEEE Transactions on Robotics*, 41:1553–1567, 2025. doi: 10.1109/TRO.2025.3539193.

648 Yao Mu, Qinglong Zhang, Mengkang Hu, Wenhui Wang, Mingyu Ding, Jun Jin, Bin Wang, Jifeng
 649 Dai, Yu Qiao, and Ping Luo. EmbodiedGPT: Vision-language pre-training via embodied chain
 650 of thought. In *Thirty-seventh Conference on Neural Information Processing Systems*, 2023. URL
 651 <https://openreview.net/forum?id=IL5zJqfxAa>.

652

653 NVIDIA, Johan Bjorck, Fernando Castañeda, Nikita Cherniadev, Xingye Da, Runyu Ding,
 654 Linxi "Jim" Fan, Yu Fang, Dieter Fox, Fengyuan Hu, Spencer Huang, Joel Jang, Zhenyu Jiang,
 655 Jan Kautz, Kaushil Kundalia, Lawrence Lao, Zhiqi Li, Zongyu Lin, Kevin Lin, Guilin Liu,
 656 Edith Llontop, Loic Magne, Ajay Mandlekar, Avnish Narayan, Soroush Nasiriany, Scott Reed,
 657 You Liang Tan, Guanzhi Wang, Zu Wang, Jing Wang, Qi Wang, Jiannan Xiang, Yuqi Xie, Yinzhen
 658 Xu, Zhenjia Xu, Seonghyeon Ye, Zhiding Yu, Ao Zhang, Hao Zhang, Yizhou Zhao, Ruijie Zheng,
 659 and Yuke Zhu. Gr00t n1: An open foundation model for generalist humanoid robots, 2025. URL
 660 <https://arxiv.org/abs/2503.14734>.

661

662 Octo Model Team, Dibya Ghosh, Homer Walke, Karl Pertsch, Kevin Black, Oier Mees, Sudeep
 663 Dasari, Joey Hejna, Charles Xu, Jianlan Luo, Tobias Kreiman, You Liang Tan, Lawrence Yunliang
 664 Chen, Pannag Sanketi, Quan Vuong, Ted Xiao, Dorsa Sadigh, Chelsea Finn, and Sergey Levine.
 665 Octo: An open-source generalist robot policy. In *Proceedings of Robotics: Science and Systems*,
 666 Delft, Netherlands, 2024.

667 OpenAI. Chatgpt-4o (may 13, 2024 version) [large language model]. <https://chat.openai.com>, 2024.

668

669 Maxime Oquab, Timothée Darcet, Théo Moutakanni, Huy Q. Vo, Marc Szafraniec, Vasil Khali-
 670 dov, Pierre Fernandez, Daniel Haziza, Francisco Massa, Alaaeldin El-Nouby, Mahmoud Ass-
 671 ran, Nicolas Ballas, Wojciech Galuba, Russ Howes, Po-Yao (Bernie) Huang, Shang-Wen Li,
 672 Ishan Misra, Michael G. Rabbat, Vasu Sharma, Gabriel Synnaeve, Huijiao Xu, Hervé Jégou,
 673 Julien Mairal, Patrick Labatut, Armand Joulin, and Piotr Bojanowski. Dinov2: Learning ro-
 674 bust visual features without supervision. *ArXiv*, abs/2304.07193, 2023. URL <https://api.semanticscholar.org/CorpusID:258170077>.

675

676 Delin Qu, Haoming Song, Qizhi Chen, Yuanqi Yao, Xinyi Ye, Yan Ding, Zhigang Wang, JiaYuan
 677 Gu, Bin Zhao, Dong Wang, and Xuelong Li. Spatialvlva: Exploring spatial representations for
 678 visual-language-action model, 2025. URL <https://arxiv.org/abs/2501.15830>.

679

680 Nikhila Ravi, Valentin Gabeur, Yuan-Ting Hu, Ronghang Hu, Chaitanya Ryali, Tengyu Ma, Haitham
 681 Khedr, Roman Rädle, Chloe Rolland, Laura Gustafson, Eric Mintun, Junting Pan, Kalyan Va-
 682 sudev Alwala, Nicolas Carion, Chao-Yuan Wu, Ross Girshick, Piotr Dollár, and Christoph Fe-
 683 ichtenhofer. Sam 2: Segment anything in images and videos, 2024. URL <https://arxiv.org/abs/2408.00714>.

684

685 Mohit Shridhar, Lucas Manuelli, and Dieter Fox. Perceiver-actor: A multi-task transformer for
 686 robotic manipulation. In *Proceedings of the 6th Conference on Robot Learning (CoRL)*, 2022.

687

688 Mustafa Shukor, Dana Aubakirova, Francesco Capuano, Pepijn Kooijmans, Steven Palma, Adil
 689 Zouitine, Michel Aractingi, Caroline Pascal, Martino Russi, Andres Marafioti, Simon Alibert,
 690 Matthieu Cord, Thomas Wolf, and Remi Cadene. Smolvla: A vision-language-action model for
 691 affordable and efficient robotics, 2025. URL <https://arxiv.org/abs/2506.01844>.

692

693 Gemini Robotics Team, Saminda Abeyruwan, Joshua Ainslie, Jean-Baptiste Alayrac, Montser-
 694 rat Gonzalez Arenas, Travis Armstrong, Ashwin Balakrishna, Robert Baruch, Maria Bauza,
 695 Michiel Blokzijl, Steven Bohez, Konstantinos Bousmalis, Anthony Brohan, Thomas Buschmann,
 696 Arunkumar Byravan, Serkan Cabi, Ken Caluwaerts, Federico Casarini, Oscar Chang, Jose En-
 697 rique Chen, Xi Chen, Hao-Tien Lewis Chiang, Krzysztof Choromanski, David D'Ambrosio,
 698 Sudeep Dasari, Todor Davchev, Coline Devin, Norman Di Palo, Tianli Ding, Adil Dostmohamed,
 699 Danny Driess, Yilun Du, Debidatta Dwibedi, Michael Elabd, Claudio Fantacci, Cody Fong, Erik
 700 Frey, Chuyuan Fu, Marissa Giustina, Keerthana Gopalakrishnan, Laura Graesser, Leonard Hasen-
 701 clever, Nicolas Heess, Brandon Hernaez, Alexander Herzog, R. Alex Hofer, Jan Humplik, Atil
 Iscen, Mithun George Jacob, Deepali Jain, Ryan Julian, Dmitry Kalashnikov, M. Emre Karago-
 zler, Stefani Karp, Chase Kew, Jerad Kirkland, Sean Kirmani, Yuheng Kuang, Thomas Lampe,
 Antoine Laurens, Isabel Leal, Alex X. Lee, Tsang-Wei Edward Lee, Jacky Liang, Yixin Lin,

702 Sharath Maddineni, Anirudha Majumdar, Assaf Hurwitz Michaely, Robert Moreno, Michael Ne-
 703 unert, Francesco Nori, Carolina Parada, Emilio Parisotto, Peter Pastor, Acorn Pooley, Kanishka
 704 Rao, Krista Reymann, Dorsa Sadigh, Stefano Saliceti, Pannag Sanketi, Pierre Sermanet, Dhruv
 705 Shah, Mohit Sharma, Kathryn Shea, Charles Shu, Vikas Sindhwani, Sumeet Singh, Radu Soricu-
 706 Jost Tobias Springenberg, Rachel Sterneck, Razvan Surdulescu, Jie Tan, Jonathan Tompson, Vin-
 707 cent Vanhoucke, Jake Varley, Grace Vesom, Giulia Vezzani, Oriol Vinyals, Ayzaan Wahid, Stefan
 708 Welker, Paul Wohlhart, Fei Xia, Ted Xiao, Annie Xie, Jinyu Xie, Peng Xu, Sichun Xu, Ying
 709 Xu, Zhuo Xu, Yuxiang Yang, Rui Yao, Sergey Yaroshenko, Wenhao Yu, Wentao Yuan, Jingwei
 710 Zhang, Tingnan Zhang, Allan Zhou, and Yuxiang Zhou. Gemini robotics: Bringing ai into the
 711 physical world, 2025. URL <https://arxiv.org/abs/2503.20020>.

712 Chenxi Wang, Hongjie Fang, Haoshu Fang, and Cewu Lu. Rise: 3d perception makes
 713 real-world robot imitation simple and effective. 2024 IEEE/RSJ International Conference
 714 on Intelligent Robots and Systems (IROS), pp. 2870–2877, 2024a. URL <https://api.semanticscholar.org/CorpusID:269214333>.

715 Yixuan Wang, Guang Yin, Binghao Huang, Tarik Kelestemur, Jiuguang Wang, and Yunzhu Li.
 716 Gendp: 3d semantic fields for category-level generalizable diffusion policy. In 8th Annual Con-
 717 ference on Robot Learning, 2024b.

718 Junjie Wen, Yichen Zhu, Jinming Li, Minjie Zhu, Kun Wu, Zhiyuan Xu, Ning Liu, Ran Cheng,
 719 Chaomin Shen, Yixin Peng, et al. Tinyvla: Towards fast, data-efficient vision-language-action
 720 models for robotic manipulation. In IEEE Robotics and Automation Letters (RA-L), 2025a.

721 Junjie Wen, Yichen Zhu, Zhibing Tang, Jinming Li, Yixin Peng, Chaomin Shen, and Feifei Feng.
 722 Dexvla: Vision-language model with plug-in diffusion expert for visuomotor policy learning.
 723 Conference on Robot Learning (CoRL), 2025b.

724 Wentao Yuan, Jiafei Duan, Valts Blukis, Wilbert Pumacay, Ranjay Krishna, Adithyavairavan Murali,
 725 Arsalan Mousavian, and Dieter Fox. Robopoint: A vision-language model for spatial affordance
 726 prediction in robotics. In 8th Annual Conference on Robot Learning, 2024. URL <https://openreview.net/forum?id=GVX6jpZOHU>.

727 Michał Zawalski, William Chen, Karl Pertsch, Oier Mees, Chelsea Finn, and Sergey Levine. Robotic
 728 control via embodied chain-of-thought reasoning. In 8th Annual Conference on Robot Learning,
 729 2024. URL <https://openreview.net/forum?id=S70MgnIA0v>.

730 Yanjie Ze, Gu Zhang, Kangning Zhang, Chenyuan Hu, Muhan Wang, and Huazhe Xu. 3d diffusion
 731 policy: Generalizable visuomotor policy learning via simple 3d representations. In Proceedings
 732 of Robotics: Science and Systems (RSS), 2024.

733 Xiaohua Zhai, Basil Mustafa, Alexander Kolesnikov, and Lucas Beyer. Sigmoid loss for language
 734 image pre-training. 2023 IEEE/CVF International Conference on Computer Vision (ICCV),
 735 pp. 11941–11952, 2023. URL <https://api.semanticscholar.org/CorpusID:257767223>.

736 Qingqing Zhao, Yao Lu, Moo Jin Kim, Zipeng Fu, Zhuoyang Zhang, Yecheng Wu, Zhaoshuo
 737 Li, Qianli Ma, Song Han, Chelsea Finn, Ankur Handa, Ming-Yu Liu, Donglai Xiang, Gor-
 738 don Wetzstein, and Tsung-Yi Lin. Cot-vla: Visual chain-of-thought reasoning for vision-
 739 language-action models. 2025 IEEE/CVF Conference on Computer Vision and Pattern Recog-
 740 nition (CVPR), pp. 1702–1713, 2025. URL <https://api.semanticscholar.org/CorpusID:277435005>.

741 Haoyu Zhen, Xiaowen Qiu, Peihao Chen, Jincheng Yang, Xin Yan, Yilun Du, Yining Hong, and
 742 Chuang Gan. 3d-vla: a 3d vision-language-action generative world model. In Proceedings of the
 743 41st International Conference on Machine Learning, ICML’24. JMLR.org, 2024.

744 Haoyi Zhu, Honghui Yang, Yating Wang, Jiange Yang, Limin Wang, and Tong He. Spa: 3d spatial-
 745 awareness enables effective embodied representation. In Y. Yue, A. Garg, N. Peng, F. Sha, and
 746 R. Yu (eds.), International Conference on Representation Learning, volume 2025, pp. 26361–
 747 26391, 2025. URL https://proceedings.iclr.cc/paper_files/paper/2025/file/421fcf51a0e243f15f977553a6f482cb-Paper-Conference.pdf.

756
757 Table 4: **Number of samples.** We record the number of samples in training set and validation set
758 for different datasets used in the simulation experiments for GemBench.

	Language Plan	Object Position	Robot Trajectory Data
Train	30515	39777	169665
Validation	6103	16650	17400

762 763 A APPENDIX

764 A.1 GEMBENCH TASK SPECIFICATION

767 The detailed tasks and variations in GemBench (Garcia et al., 2025) used for training and evaluation
768 are listed in Table 5.

770 A.2 TRAINING DATA SPECIFICATION

772 We have three datasets in total for finetuning the pre-trained VLM: a language plan dataset, a object
773 position dataset and a robot trajectory dataset.

- 775 • For language plan dataset, we label each task with a language plan according to the decom-
776 position of the task. Note that one task may contain different variations. Each variation of
777 the task is assigned with a different language plan. We augment the data by asking LLM to
778 provide some variations on the language descriptions of the plan.
- 779 • For object position dataset, we randomly initialize the scene of the tasks and apply trans-
780 formations (translation and rotation) on the scene. We record the RGB-D images along with
781 the 3D positions of the objects. The 3D positions of the objects are projected into canonical
782 views to obtain the pixel positions in each view.
- 783 • For robot trajectory dataset, we explain in the Section 5.1 on how we sample transitions
784 from the demonstrations to build observation-action pair. Transformations (translation and
785 rotation) are also applied on the transitions to augment the data.

786 In practice, the number of training samples for each dataset used for GemBench is listed in Table 4.

788 A.3 EXPERIMENTAL DETAILS

790 All experiments are conducted on 4 NVIDIA RTX 4090 GPU. The hyperparameters and training
791 time are listed in Table 6.

793 A.4 GEMBENCH SUCCESS RATE PER TASK

794 The results for each task across different generalization levels in Gembench are listed in Table 7,
795 Table 8, Table 9, Table 10.

797 A.5 ADDITIONAL ABLATION STUDY

799 We first show the performance of our method on GemBench trained with different numbers of robot
800 trajectories (10, 20, 50, 100) in Table 11. Further increasing the number of robot trajectory improves
801 on the in-domain performance (L1) while does not help in the average success rate. We conclude
802 that the data efficiency is attributed to the following points.

- 804 • Task decomposition allows the agent to learn common skills among different tasks and
805 allows compositional generalization.
- 806 • Bridging VLM and 3D manipulation with projected images, separating task planning from
807 keypoint prediction, and Chain-of-Thought reasoning lead to an effective adaptation of
808 pre-trained VLM to the coarse task planner.
- 809 • Data efficiency with respect to the robot trajectories also benefits from leveraging language
plans and object position data. By co-training on these additional sources, our framework

Table 5: Training and evaluation tasks & variations in GemBench. The evaluation tasks contain four levels of generalization, where Level 1 evaluates the generalization to novel placements, Level 2 novel rigid objects, Level 3 novel articulated objects, and Level 4 novel long-horizon tasks.

		Train / Level 1		Level 2		Level 3		Level 4
Task		Variation	Color	Shape	Instance	Category	Action-Part	Long-horizon
Press	Push button	maroon button navy button yellow button	azure button rose button white button	Lamp on				2 buttons 3 buttons 4 buttons
Pick	Pick and lift	red block lime block cyan block magenta cup silver cup orange cup	teal block violet block black block gray cup olive cup purple cup	red cylinder red star red moon				
	Pick up cup			red toy				
	Slide block	green target blue target teal target	pink target yellow target cyan target					
Push	Reach and drag	black target	navy target					
	Close jar	azule jar violet jar rose bulb white bulb	blue jar green jar lime bulb maroon bulb					
Screw	Screw bulb							
	Close fridge	fridge		fridge2				
	Close laptop lid	laptop lid		laptop lid2				
Close	Close microwave	microwave		microwave2				
	Open door	door		door2				
	Open box	box		box2				
	Open drawer	bottom drawer top drawer		drawer2, drawer3 long drawer w/ 4 levels		toilet	fridge laptop lid microwave middle drawer	Take shoes out of box Put 3 items in drawer
Open	Stack blocks	2 gray blocks 2 olive blocks 2 purple blocks	2 orange blocks 2 silver blocks 2 magenta blocks					Stack 3-4 blocks Stack 2 cups
	Put groceries	crackers box soup can		mustard bottle sugar box				Put all groceries
	Put money	bottom shelf middle shelf		Put cube in bottom shelf				top shelf

Table 6: **Training time and hyperparameters used in different experiments.** Here we list the training time and hyperparameters used for training the model with GemBench and real-world data.

	GemBench		Real-world	
	Coarse task planner	Fine-grained Action Predictor	Coarse task planner	Fine-grained Action Predictor
Training time	6 hours	3 hours	1 hour	1 hour
Learning rate	3e-4	0.0024	1e-4	0.0024
Batch Size	64	192	64	192
Epochs	1	5	1	3
Lora Rank	8	/	8	/
Lora Alpha	32	/	32	/
Freeze ViT	False	/	False	/
Freeze Aligner	True	/	True	/
Freeze LLM	False	/	False	/

equips the model with task-planning and object-grounding abilities, leaving it to learn only how to act given sub-task instructions and known object locations. In contrast, prior approaches required the model to learn task planning, object detection, and action prediction solely from robot trajectories.

We then show the results of variations on inputs to the fine-grained action predictor in Table 12. Removing some components in the fine-grained action predictor leads to performance drop to some extend.

A.6 REAL-WORLD EXPERIMENTS

An overview of the tasks used in real-world experiments are shown in Figure 4.

864	Method	Avg.	Close Fridge+0	Close Jar+15	Close Jar+16	CloseLaptop Lid+0	Close Microwave+0	LightBulb In+17	LightBulb In+19	Open Box+0	Open Door+0	Open Drawer+0
865	HiveFormer (Guhur et al., 2023)	60.3 \pm 1.5	98 \pm 4.2	64 \pm 13.9	92 \pm 2.7	90 \pm 3.5	88 \pm 7.6	12 \pm 4.5	13 \pm 6.7	4 \pm 4.2	53 \pm 15.2	15 \pm 12.2
866	PolarNet (Chen et al., 2023)	77.6 \pm 0.9	99 \pm 2.2	99 \pm 2.2	99 \pm 2.2	95 \pm 3.5	98 \pm 2.7	72 \pm 12.5	71 \pm 6.5	32 \pm 11.5	69 \pm 8.9	61 \pm 12.4
867	3D Diffuser Actor (Ke et al., 2024)	91.9 \pm 0.8	100 \pm 0.0	100 \pm 0.0	100 \pm 0.0	99 \pm 2.2	100 \pm 0.0	85 \pm 5.0	88 \pm 2.7	11 \pm 2.2	96 \pm 4.2	82 \pm 9.1
868	RVT2 (Goyal et al., 2024)	89.0 \pm 0.8	77 \pm 11.0	97 \pm 4.5	98 \pm 2.7	77 \pm 13.0	100 \pm 0.0	93 \pm 5.7	91 \pm 8.2	7 \pm 4.5	98 \pm 4.5	93 \pm 5.7
869	3D-LOTUS (Garcia et al., 2025)	94.3 \pm 3.5	96 \pm 3.7	100 \pm 0.0	100 \pm 0.0	98 \pm 2.5	98 \pm 4.0	84 \pm 7.4	85 \pm 9.5	99 \pm 2.0	77 \pm 9.5	83 \pm 8.7
870	3D-LOTUS++ (Garcia et al., 2025)	68.7 \pm 0.6	95 \pm 0.0	100 \pm 0.0	99 \pm 2.0	28 \pm 2.5	87 \pm 5.1	55 \pm 10.5	45 \pm 8.9	55 \pm 8.9	79 \pm 9.7	68 \pm 12.5
871	BridgeVLA (Li et al., 2025b)	91.1 \pm 1.1	99 \pm 2.0	98 \pm 4.0	100 \pm 0.0	97 \pm 2.5	85 \pm 5.5	90 \pm 5.5	87 \pm 7.5	76 \pm 10.2	70 \pm 12.3	86 \pm 5.8
872	CLAP	83.9 \pm 0.3	88 \pm 4.5	98 \pm 2.7	100 \pm 0.0	88 \pm 9.1	99 \pm 2.2	84 \pm 6.5	76 \pm 9.1	17 \pm 5.7	82 \pm 4.5	87 \pm 15.0
873	Method	Open Drawer+2	Pick& Lift+0	Pick& Lift+2	Pick& Lift+7	PickUp Cup+9	PickUp Cup+9	PickUp Cup+11	Push Button+0	Push Button+3	Push Button+4	Push Cupboard+0
874	HiveFormer (Guhur et al., 2023)	59 \pm 7.4	86 \pm 4.2	92 \pm 6.7	93 \pm 2.7	83 \pm 7.6	69 \pm 12.9	61 \pm 19.8	84 \pm 11.9	68 \pm 6.7	87 \pm 7.6	34 \pm 8.2
875	PolarNet (Chen et al., 2023)	90 \pm 7.1	92 \pm 9.1	84 \pm 7.4	88 \pm 5.7	82 \pm 7.6	79 \pm 14.2	72 \pm 10.4	100 \pm 0.0	99 \pm 2.2	52 \pm 7.6	52 \pm 7.6
876	3D Diffuser Actor (Ke et al., 2024)	97 \pm 4.5	99 \pm 2.2	99 \pm 2.2	99 \pm 2.2	96 \pm 2.2	97 \pm 4.5	98 \pm 2.7	98 \pm 2.7	96 \pm 4.2	98 \pm 2.7	85 \pm 5.0
877	RVT2 (Goyal et al., 2024)	94 \pm 4.2	99 \pm 2.2	98 \pm 2.7	100 \pm 0.0	99 \pm 2.2	99 \pm 2.2	100 \pm 0.0	100 \pm 0.0	100 \pm 0.0	100 \pm 0.0	88 \pm 8.4
878	3D-LOTUS (Garcia et al., 2025)	93 \pm 6.0	99 \pm 2.0	100 \pm 0.0	99 \pm 2.0	97 \pm 4.0	96 \pm 3.7	94 \pm 4.9	99 \pm 2.0	100 \pm 0.0	100 \pm 0.0	89 \pm 5.8
879	3D-LOTUS++ (Garcia et al., 2025)	75 \pm 4.5	97 \pm 6.0	94 \pm 3.7	93 \pm 5.1	86 \pm 8.0	88 \pm 6.8	91 \pm 4.9	100 \pm 0.0	100 \pm 0.0	100 \pm 0.0	1 \pm 2.0
880	BridgeVLA (Li et al., 2025b)	99 \pm 2.0	99 \pm 2.0	100 \pm 0.0	98 \pm 2.5	96 \pm 2.0	94 \pm 3.7	99 \pm 2.0	100 \pm 0.0	98 \pm 4.0	95 \pm 4.0	74 \pm 6.6
881	CLAP	98 \pm 2.7	98 \pm 2.7	99 \pm 2.2	99 \pm 2.2	94 \pm 5.5	99 \pm 2.2	93 \pm 7.6	100 \pm 0.0	100 \pm 0.0	97 \pm 2.7	58 \pm 10.4
882	Method	PutIn Cupboard+3	PutMoney InSafe+0	PutMoney InSafe+1	Reach& Drag+14	Reach& Drag+18	Slide Block+0	Slide Block+1	Stack Blocks+30	Stack Blocks+30	Stack Blocks+30	Stack Blocks+30
883	HiveFormer (Guhur et al., 2023)	74 \pm 6.5	85 \pm 3.5	88 \pm 2.7	37 \pm 5.7	32 \pm 7.6	99 \pm 2.2	91 \pm 12.4	64 \pm 5.5	7 \pm 4.5	6 \pm 4.2	6 \pm 4.2
884	PolarNet (Chen et al., 2023)	88 \pm 4.5	95 \pm 4.5	95 \pm 5.0	99 \pm 2.2	100 \pm 0.0	0 \pm 0.0	34 \pm 10.8	30 \pm 9.4	36 \pm 12.9	30 \pm 9.4	30 \pm 9.4
885	3D Diffuser Actor (Ke et al., 2024)	82 \pm 11.5	95 \pm 5.0	98 \pm 2.7	100 \pm 0.0	99 \pm 2.2	100 \pm 0.0	89 \pm 4.2	88 \pm 7.6	85 \pm 6.1	89 \pm 5.5	89 \pm 5.5
886	RVT2 (Goyal et al., 2024)	80 \pm 6.1	95 \pm 8.4	96 \pm 8.5	85 \pm 10.0	94 \pm 2.2	100 \pm 0.0	37 \pm 6.7	88 \pm 5.7	93 \pm 2.7	88 \pm 11.5	88 \pm 11.5
887	3D-LOTUS (Garcia et al., 2025)	72 \pm 11.2	94 \pm 3.7	99 \pm 2.0	99 \pm 2.0	99 \pm 2.0	100 \pm 0.0	100 \pm 0.0	94 \pm 5.8	91 \pm 6.6	90 \pm 4.5	90 \pm 4.5
888	3D-LOTUS++ (Garcia et al., 2025)	2 \pm 2.5	22 \pm 6.8	16 \pm 4.9	94 \pm 3.7	62 \pm 8.7	100 \pm 0.0	65 \pm 5.5	86 \pm 5.8	20 \pm 4.5	28 \pm 13.6	28 \pm 13.6
889	BridgeVLA (Li et al., 2025b)	84 \pm 6.6	79 \pm 9.7	86 \pm 3.7	96 \pm 5.8	97 \pm 4.0	100 \pm 0.0	90 \pm 5.5	77 \pm 8.1	87 \pm 4.0	85 \pm 7.8	85 \pm 7.8
890	CLAP	69 \pm 12.4	80 \pm 6.1	82 \pm 7.6	90 \pm 3.5	90 \pm 34.5	55 \pm 5.0	3 \pm 5.0	96 \pm 4.2	85 \pm 3.5	90 \pm 6.1	90 \pm 6.1
891	Method	Stack Blocks+24	Stack Blocks+24	Stack Blocks+33	Stack Blocks+33	Slide Block+2	Slide Block+3	Close Jar+3	Close Jar+4	LightBulb In+1	LightBulb In+2	Lamp Lamp On+0
892	HiveFormer (Guhur et al., 2023)	0 \pm 0.0	4 \pm 4.2	0 \pm 0.0	0 \pm 0.0	0 \pm 0.0	0 \pm 0.0	0 \pm 0.0	4 \pm 4.2	0 \pm 0.0	7 \pm 4.5	7 \pm 4.5
893	PolarNet (Chen et al., 2023)	1 \pm 2.2	2 \pm 2.7	6 \pm 8.2	0 \pm 0.0	0 \pm 0.0	20 \pm 10.6	82 \pm 5.7	22 \pm 11.5	17 \pm 8.4	14 \pm 10.8	14 \pm 10.8
894	3D Diffuser Actor (Ke et al., 2024)	66 \pm 13.9	82 \pm 2.7	50 \pm 14.6	0 \pm 0.0	0 \pm 0.0	23 \pm 16.8	82 \pm 5.7	51 \pm 17.8	60 \pm 10.0	7 \pm 7.6	7 \pm 7.6
895	RVT2 (Goyal et al., 2024)	18 \pm 4.5	56 \pm 16.7	45 \pm 13.7	0 \pm 0.0	1 \pm 2.2	7 \pm 7.6	77 \pm 5.7	68 \pm 14.4	6 \pm 6.5	0 \pm 0.0	0 \pm 0.0
896	3D-LOTUS (Garcia et al., 2025)	13 \pm 8.1	40 \pm 9.5	69 \pm 5.8	0 \pm 0.0	0 \pm 0.0	71 \pm 5.8	90 \pm 4.5	24 \pm 4.9	41 \pm 8.6	0 \pm 0.0	0 \pm 0.0
897	3D-LOTUS++ (Garcia et al., 2025)	22 \pm 9.3	83 \pm 7.5	59 \pm 3.7	27 \pm 9.8	5 \pm 3.2	98 \pm 2.5	96 \pm 3.7	56 \pm 9.7	43 \pm 7.5	2 \pm 2.0	2 \pm 2.0
898	BridgeVLA (Li et al., 2025b)	61 \pm 10.7	51 \pm 13.2	79 \pm 8.6	12 \pm 9.3	3 \pm 4.0	66 \pm 6.6	88 \pm 4.0	66 \pm 8.6	74 \pm 5.8	7 \pm 4.0	7 \pm 4.0
899	CLAP	95 \pm 3.5	86 \pm 2.2	91 \pm 4.2	18 \pm 5.7	68 \pm 7.7	95 \pm 3.5	98 \pm 4.5	60 \pm 5.5	81 \pm 6.5	20 \pm 6.1	20 \pm 6.1
900	Method	Reach& Drag+5	Reach& Drag+7	PutCub InSafe+0	Pick&Lift Cylinder+0	Pick&Lift Star+0	Pick&Lift Moon+0	Pick&Lift Toy+0	PutIn Cupboard+7	PutIn Cupboard+8		
901	HiveFormer (Guhur et al., 2023)	1 \pm 2.2	0 \pm 0.0	4 \pm 2.2	78 \pm 5.7	73 \pm 7.6	88 \pm 2.7	87 \pm 4.5	0 \pm 0.0	0 \pm 0.0	0 \pm 0.0	0 \pm 0.0
902	PolarNet (Chen et al., 2023)	61 \pm 8.2	10 \pm 6.1	40 \pm 14.1	93 \pm 6.7	88 \pm 8.4	93 \pm 6.7	90 \pm 3.5	0 \pm 0.0	0 \pm 0.0	0 \pm 0.0	0 \pm 0.0
903	3D Diffuser Actor (Ke et al., 2024)	0 \pm 0.0	64 \pm 6.5	3 \pm 2.7	99 \pm 2.2	43 \pm 17.9	91 \pm 9.6	30 \pm 9.4	0 \pm 0.0	0 \pm 0.0	3 \pm 4.5	3 \pm 4.5
904	RVT2 (Goyal et al., 2024)	91 \pm 2.2	89 \pm 6.5	6 \pm 5.5	98 \pm 2.7	98 \pm 4.5	94 \pm 4.2	78 \pm 8.4	0 \pm 0.0	0 \pm 0.0	0 \pm 0.0	0 \pm 0.0
905	3D-LOTUS (Garcia et al., 2025)	95 \pm 4.5	18 \pm 10.8	25 \pm 5.5	88 \pm 8.7	69 \pm 6.6	80 \pm 8.4	96 \pm 3.7	0 \pm 0.0	0 \pm 0.0	0 \pm 0.0	0 \pm 0.0
906	3D-LOTUS++ (Garcia et al., 2025)	94 \pm 2.0	64 \pm 12.4	37 \pm 5.1	91 \pm 2.0	94 \pm 3.7	29 \pm 6.6	71 \pm 2.0	1 \pm 2.0	0 \pm 0.0	0 \pm 0.0	0 \pm 0.0
907	BridgeVLA (Li et al., 2025b)	94 \pm 3.7	96 \pm 3.7	3 \pm 2.5	98 \pm 2.5	99 \pm 2.0	95 \pm 3.2	93 \pm 5.1	0 \pm 0.0	0 \pm 0.0	0 \pm 0.0	0 \pm 0.0
908	CLAP	95 \pm 3.5	90 \pm 6.1	61 \pm 14.7	97 \pm 2.7	100 \pm 0.0	98 \pm 2.7	84 \pm 8.2	50 \pm 11.2	53 \pm 12.5		

Table 7: Per-task Success Rate on GemBench Level 1.

Examples of Real-world Tasks

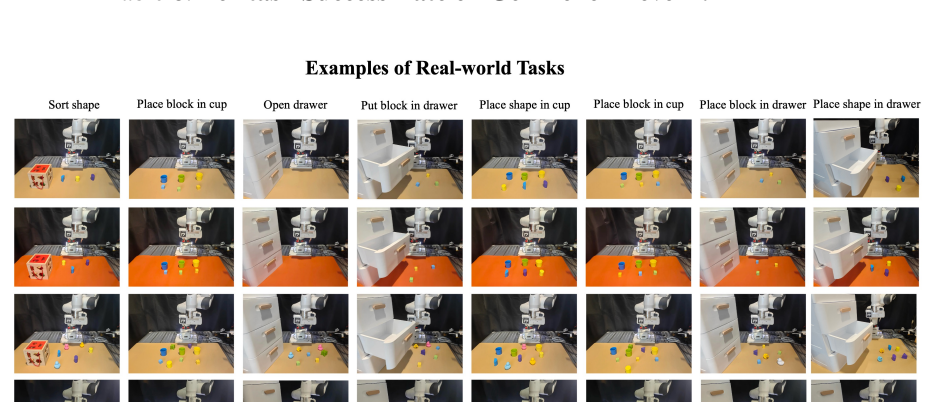


Figure 4: Overview of the evaluation tasks in real-world experiments. We evaluate the all these eight tasks across different variations and record the success rate.

Method	Avg.	Close Door+0	Close Box+0	Close Fridge+2+0	CloseLaptop Lid+0	Close Microwave+2+0	Open Door+2+0	Open Box+2+0
HiveFormer (Guhur et al., 2023)	35.1 ± 1.7	0 ± 0.0	1 ± 2.2	34 ± 9.6	52 ± 9.1	15 ± 7.1	32 ± 11.5	5 ± 3.5
PolarNet (Chen et al., 2023)	38.5 ± 1.7	0 ± 0.0	0 ± 0.0	78 ± 5.7	26 ± 8.2	74 ± 6.5	33 ± 6.7	23 ± 8.4
3D Diffuser Actor (Ke et al., 2024)	37.0 ± 2.2	0 ± 0.0	0 ± 0.0	97 ± 2.7	23 ± 6.7	88 ± 7.6	86 ± 7.4	67 ± 8.8
RVT2 (Goyal et al., 2024)	36.0 ± 2.2	1 ± 2.2	2 ± 2.7	72 ± 6.7	42 ± 14.0	71 ± 8.9	79 ± 6.5	5 ± 6.1
3D-LOTUS (Garcia et al., 2025)	38.1 ± 1.1	0 ± 0.0	58 ± 8.1	36 ± 9.7	54 ± 10.7	85 ± 7.1	42 ± 6.8	11 ± 6.6
3D-LOTUS++ (Garcia et al., 2025)	41.5 ± 1.8	1 ± 2.0	29 ± 8.6	93 ± 2.5	50 ± 9.5	99 ± 2.0	52 ± 10.3	16 ± 8.0
BridgeVLA (Li et al., 2025b)	43.8 ± 1.2	0 ± 0.0	1 ± 2.0	95 ± 5.5	77 ± 4.0	54 ± 10.2	68 ± 10.8	74 ± 4.9
CLAP	49.6 ± 2.1	3 ± 2.7	9 ± 5.5	92 ± 4.5	35 ± 9.4	79 ± 5.5	56 ± 6.5	1 ± 2.2
Method	Open Drawer+2+0	Open Drawer+3+0	OpenDrawer Long+0	OpenDrawer Long+1	OpenDrawer Long+2	OpenDrawer Long+3	Toilet SeatUp+0	Open Fridge+0
HiveFormer (Guhur et al., 2023)	59 ± 11.9	39 ± 11.9	78 ± 8.4	82 ± 4.5	49 ± 4.2	57 ± 11.5	6 ± 4.2	0 ± 0.0
PolarNet (Chen et al., 2023)	91 ± 4.2	29 ± 8.2	84 ± 11.9	88 ± 5.7	63 ± 8.4	37 ± 7.6	2 ± 2.7	4 ± 2.2
3D Diffuser Actor (Ke et al., 2024)	19 ± 8.2	1 ± 2.2	15 ± 5.0	35 ± 13.7	26 ± 9.6	79 ± 12.9	0 ± 0.0	7 ± 5.7
RVT2 (Goyal et al., 2024)	81 ± 11.9	0 ± 0.0	84 ± 8.2	39 ± 10.8	11 ± 8.9	75 ± 6.1	7 ± 5.7	0 ± 0.0
3D-LOTUS (Garcia et al., 2025)	90 ± 3.2	22 ± 8.1	56 ± 13.9	33 ± 11.2	17 ± 8.1	75 ± 6.3	0 ± 0.0	4 ± 5.8
3D-LOTUS++ (Garcia et al., 2025)	70 ± 5.5	41 ± 4.9	72 ± 4.0	52 ± 10.8	23 ± 8.1	78 ± 5.1	8 ± 5.1	0 ± 0.0
BridgeVLA (Li et al., 2025b)	65 ± 6.3	87 ± 6.0	59 ± 8.6	34 ± 8.0	18 ± 10.3	85 ± 8.4	6 ± 5.8	7 ± 2.5
CLAP	68 ± 8.4	87 ± 7.6	44 ± 10.8	94 ± 5.5	14 ± 5.5	76 ± 13.4	7 ± 4.5	3 ± 4.5
Method	OpenLaptop Lid+0	Open Microwave+0	PutMoney InSafe+2	Open Drawer+1	Close Drawer+0	Close Grill+0		
HiveFormer (Guhur et al., 2023)	100 ± 0.0	0 ± 0.0	0 ± 0.0	0 ± 0.0	83 ± 5.7	44 ± 10.8		
PolarNet (Chen et al., 2023)	100 ± 0.0	0 ± 0.0	1 ± 2.2	4 ± 4.2	29 ± 11.9	42 ± 11.5		
3D Diffuser Actor (Ke et al., 2024)	100 ± 0.0	0 ± 0.0	2 ± 4.5	0 ± 0.0	66 ± 7.4	65 ± 13.7		
RVT2 (Goyal et al., 2024)	93 ± 5.7	0 ± 0.0	0 ± 0.0	6 ± 2.2	78 ± 8.4	9 ± 4.2		
3D-LOTUS (Garcia et al., 2025)	100 ± 0.0	0 ± 0.0	0 ± 0.0	0 ± 0.0	87 ± 8.1	29 ± 6.6		
3D-LOTUS++ (Garcia et al., 2025)	86 ± 6.6	0 ± 0.0	13 ± 8.1	0 ± 0.0	69 ± 5.8	19 ± 13.9		
BridgeVLA (Li et al., 2025b)	95 ± 0.0	0 ± 0.0	2 ± 2.5	0 ± 0.0	58 ± 12.9	35 ± 12.3		
CLAP	78 ± 9.1	0 ± 0.0	76 ± 5.5	96 ± 6.5	84 ± 8.2	40 ± 7.1		

Table 9: Per-task Success Rate on GemBench Level 3.

Method	Avg.	Push Buttons4+1	Push Buttons4+2	Push Buttons4+3	TakeShoes OutOfBox+0	PutItems InDrawer+0	PutItems InDrawer+2
HiveFormer (Guhur et al., 2023)	0 ± 0.0	0 ± 0.0	0 ± 0.0	0 ± 0.0	0 ± 0.0	0 ± 0.0	0 ± 0.0
PolarNet (Chen et al., 2023)	0.1 ± 0.2	1 ± 2.2	0 ± 0.0	0 ± 0.0	0 ± 0.0	0 ± 0.0	0 ± 0.0
3D Diffuser Actor (Ke et al., 2024)	0 ± 0.0	0 ± 0.0	0 ± 0.0	0 ± 0.0	0 ± 0.0	0 ± 0.0	0 ± 0.0
RVT2 (Goyal et al., 2024)	0 ± 0.0	0 ± 0.0	0 ± 0.0	0 ± 0.0	0 ± 0.0	0 ± 0.0	0 ± 0.0
3D-LOTUS (Garcia et al., 2025)	0.3 ± 0.3	3 ± 4.0	0 ± 0.0	0 ± 0.0	0 ± 0.0	0 ± 0.0	0 ± 0.0
3D-LOTUS++ (Garcia et al., 2025)	17.4 ± 0.4	76 ± 7.4	49 ± 8.6	37 ± 8.1	0 ± 0.0	0 ± 0.0	0 ± 0.0
BridgeVLA (Li et al., 2025b)	0 ± 0.0	0 ± 0.0	0 ± 0.0	0 ± 0.0	0 ± 0.0	0 ± 0.0	0 ± 0.0
CLAP	31.4 ± 0.6	98 ± 2.7	87 ± 4.5	92 ± 5.7	0 ± 0.0	0 ± 0.0	0 ± 0.0
Method	PutItems InDrawer+4	Tower4+1	Tower4+3	Stack Cups+0	Stack Cups+3	PutAllGroceries InCupboard+0	
HiveFormer (Guhur et al., 2023)	0 ± 0.0	0 ± 0.0	0 ± 0.0	0 ± 0.0	0 ± 0.0	0 ± 0.0	
PolarNet (Chen et al., 2023)	0 ± 0.0	0 ± 0.0	0 ± 0.0	0 ± 0.0	0 ± 0.0	0 ± 0.0	
3D Diffuser Actor (Ke et al., 2024)	0 ± 0.0	0 ± 0.0	0 ± 0.0	0 ± 0.0	0 ± 0.0	0 ± 0.0	
RVT2 (Goyal et al., 2024)	0 ± 0.0	0 ± 0.0	0 ± 0.0	0 ± 0.0	0 ± 0.0	0 ± 0.0	
3D-LOTUS (Garcia et al., 2025)	0 ± 0.0	0 ± 0.0	0 ± 0.0	0 ± 0.0	0 ± 0.0	0 ± 0.0	
3D-LOTUS++ (Garcia et al., 2025)	0 ± 0.0	17 ± 10.8	30 ± 13.4	0 ± 0.0	0 ± 0.0	0 ± 0.0	
BridgeVLA (Li et al., 2025b)	0 ± 0.0	0 ± 0.0	0 ± 0.0	0 ± 0.0	0 ± 0.0	0 ± 0.0	
CLAP	0 ± 0.0	30 ± 7.1	70 ± 6.1	0 ± 0.0	0 ± 0.0	0 ± 0.0	

Table 10: Per-task Success Rate on GemBench Level 4.

Table 11: Ablation on number of robot demonstrations used for training. We compare the results of training our method with different numbers of demonstrations. The results are recorded with three runs of different random seeds.

Number of Demos	L1	L2	L3	L4	Average
10	84.5 ± 0.8	81.5 ± 0.6	43.3 ± 1.9	30.5 ± 2.1	60.0 ± 0.1
20	83.9 ± 0.3	83.2 ± 1.9	49.6 ± 2.1	31.4 ± 0.6	62.0 ± 0.5
50	87.9 ± 0.3	81.2 ± 0.1	47.0 ± 1.5	28.3 ± 2.2	61.1 ± 0.9
100	86.9 ± 1.5	81.7 ± 0.4	47.8 ± 2.6	27.5 ± 1.2	61.0 ± 0.7

Table 12: Ablation on inputs to Fine-grained Action Predictor. We compare the results of removing some inputs to our fine-grained action predictor. The results are recorded with three runs of different random seeds.

Inputs	L1	L2	L3	L4	Average
RGB	83.9 ± 1.4	79.7 ± 2.3	48.2 ± 1.3	31.8 ± 1.3	60.9 ± 0.6
RGB+Depth	87.2 ± 2.3	83.4 ± 1.0	48.2 ± 1.0	24.3 ± 0.9	60.8 ± 0.6
RGB+Depth+3D positional embedding (Ours)	83.9 ± 0.3	83.2 ± 1.9	49.6 ± 2.1	31.4 ± 0.6	62.0 ± 0.5